Chapter 2

Experimental Techniques and Analysis Methods

2.1 Introduction

Investigating the nuclear structure at high spin requires the use of specialized techniques. In this chapter, I will discuss the process of populating high spin states in atomic nuclei, along with a detailed overview of the experiments and the setup employed in this thesis work.

2.2 Population of High Angular Momentum States in Nuclei

To investigate the diverse aspects of nuclei at high spin, specialized techniques are necessary to populate the desired isotopes through appropriate reaction channels. Subsequently, the excited nuclei de-excite via particle evaporation and gamma-ray emission. The detection of the resulting evaporated particles or gamma photons provides insights into various

properties of nuclear structure. This chapter outlines several efficient techniques employed to populate these nuclei, which will be applied within the scope of the thesis work. One of the most common methods for populating highly energetic nuclei at high angular momentum is through fusion-evaporation reactions. It involves the interaction of two stable nuclei above the Coulomb barrier. This efficient method strikes a balance between high angular momentum and a large reaction cross-section [47]. The reaction mode depends on the impact parameter. A large impact parameter b leads to Coulomb scattering, whereas partial overlap may lead to inelastic scattering. However, complete overlap results in the formation of a compound nucleus. Classically, the maximum angular momentum, l_{max}, is proportional to the projectile's momentum: $l_{max} = m_P v_P$.

In the laboratory frame, Coulomb barrier V_{coul} is given by [48] :

$$V_{coul} = \frac{(A_P + A_T)}{A_T} \frac{1.44 Z_P Z_T}{1.2(A_P^{1/3} + A_T^{1/3} + 2)}, \tag{2.1}$$

where A and Z represent mass and atomic number with the subscripts P and T specifying the projectile and target, respectively. Therefore, the excitation energy, E_{exc}, attained by the compound nucleus is given by :

$$E_{exc} = \frac{A_T}{A_T + A_P} E_{projectile} + Q, \tag{2.2}$$

where $E_{projectile}$ is the kinetic energy of the projectile and Q is the energy released owing to the difference in the final and initial masses. The first term is energy in the center of mass frame, E_{cm}. The maximum angular momentum of the compound system can be calculated as :

$$l_{max}^2 = \frac{2\mu R^2}{\hbar^2}(E_{cm} - V_{coul(cm)}), \tag{2.3}$$

where μ is the reduced mass of the system, given by $\mu = \frac{A_T A_P}{A_T + A_P}$. The recoiled distance of the closest approach is shown by R and may be approximated as the sum of the radii of the

projectile (R_P) and target (R_T). The above sets of equations constitute the whole process of compound nucleus formation which was first suggested by Niels Bohr [49] and later on experimentally verified by S. N. Ghoshal [50].

The entire process occurs within 10^{-22} to 10^{-20} seconds. During the time when the nucleus gets just formed, it spins rapidly with its spin vector perpendicular to the beam axis. Initially, the de-excitation happens through particle evaporation, like alpha particles, neutrons, and protons, until the excitation energy falls below the binding energy of a single nucleon. The time scale of this process is typically within about 10^{-16} seconds. Because of the Coulomb energy barrier, neutron emission is favored over charged particle evaporation, with each emitted particle carrying away about 8 MeV of excitation energy and extracting low angular momentum of around 1 to $2\hbar$. Once the excitation energy decreases below the threshold for particle evaporation, gamma-ray emission takes over, occurring within roughly 10^{-14} seconds (see Fig. 2.1). Fig. 2.2 shows a schematic of the decay process.

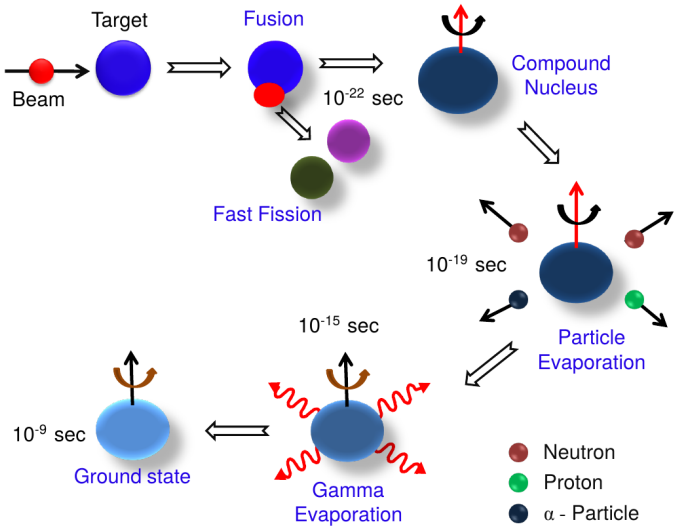

Figure 2.1 Schematic diagram illustrating the various modes of formation and decay of a compound nucleus. The Figure taken from Ref. [1]

.

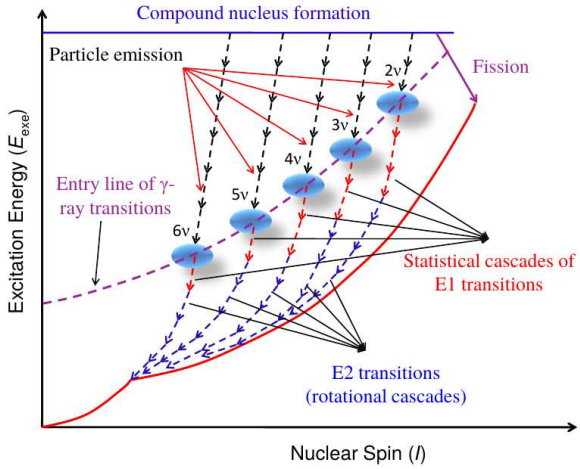

Figure 2.2 Schematic illustration of high spin residual nuclear isotope from decay of compound nucleus. The Figure taken from Ref. [1]

At first, γ ray emission occurs predominantly through statistical γ rays, primarily through $E1$ transitions. These γ rays are typically not resolved in γ-ray spectroscopy experiments. As the nucleus cools down, it gradually reaches the "yrast state" thats defines the sequence of states with the lowest energy for any given angular momentum. We observe cascade or discrete γ-ray transitions up until the nucleus arrives at its ground state. These are mostly collective $E2$ rotational cascades in the case of deformed nuclei. At times rotational dynamics may lead to $M1$ rotational cascades. A comprehensive illustration of the complete decay process of the compound nucleus is shown in Figure 2.2. Within about 10^{-9} seconds, the total decay process is completed.

The advantage of the heavy-ion fusion reaction is that it can impart very high angular momentum to the excited nucleus. A proper projectile target combination is chosen to populate desired output channels, and the bombarding energy of the projectile can be tuned to enhance some of the decay channels. In a heavy-ion reaction, the residual nuclei are aligned with their spin direction in a plane perpendicular to the beam axis. This is helpful in determining the multipolarity of γ rays. The formation and decay of compound nuclei can be effectively studied in the framework of the statistical model [51]. The effect of angular

momentum, excitation energy, shell effects etc., can also be estimated. Several packages like PACE4 [52] and CASCADE [53] are available for calculating theoretical fusion-evaporation cross-sections in reactions. The variation of calculated reaction cross section with bombarding energy for one of the reactions (^{80}Se(^{18}O, p5n)^{92}Nb) and (^{80}Se(^{18}O, p4n)^{93}Nb) using INGA spectrometer; discussed in Chapter 4 and 5 respectively) is used in this thesis.

2.3 Gamma-Ray Detection

Detecting the gamma rays emitted from excited nuclei helps determine the nuclear energy levels. To measure the energy of gamma rays in a detector, γ rays need to lose energy within the detector material. Gamma rays interact with matter differently than charged particles. There are three main ways gamma rays interact with matter: the Photoelectric effect, Compton Scattering, and Pair Production.

Photoelectric Process

This is the process where γ photons deposit the whole of their energy E_γ into the matter. The γ-ray energy in turn gets transformed into the kinetic energy of electrons, E_e :

$$E_e = E_\gamma - E_B. \tag{2.4}$$

where E_B is the binding energy of the atomic electrons. The process demands that the electrons be in a bound state within the atom in order to fulfil the laws of conservation of energy and momentum. A rough approximation for the photoelectric cross section is given empirically by :

$$\sigma_p \propto \frac{Z^n}{E_\gamma^{3.5}}. \tag{2.5}$$

Thus, the dependence of cross section on n ($4 \leq n \leq 5$) of the atomic number Z of material shows that high-Z materials are preferable for the fabrication of detectors. The process is predominant in a region with $E_\gamma < 0.3$ MeV.

Compton Effect

The effect comes into play when a γ-ray photon is elastically scattered by a free electron. Given the scattering angle of a photon to be θ, the scattered energy is given by :

$$E'_\gamma = \frac{m_e c^2}{1 - \cos\theta + \frac{m_e c^2}{E_\gamma}}, \tag{2.6}$$

where m_e is the rest mass of the recoiled electron ($m_e c^2$ = 0.511 MeV). The process results in partial deposition of incident energy into the material medium and thus is responsible for the continuous background, known as *Compton Continuum* in the energy spectrum. The Compton-scattering cross-section is approximated to be:

$$\sigma_c \propto \frac{Z}{E_\gamma}. \tag{2.7}$$

The effect is dominant for γ rays with intermediate energy.

Pair Production

A high energy photon, typically with an incident energy $> 2m_e c^2$, interacts with matter through pair production. The process leads to the formation of an electron-positron pair with both particles sharing an equal amount of incident energy. The Positron, being an anti-particle of the electron, immediately annihilates with a surrounding electron, producing two photons each moving in an opposite direction with energy 0.511 MeV. The process becomes predominant for $E_\gamma > 5.0$ MeV.

2.4 Multi-Detector Arrays

Over the past several years, significant advancements have been made in the field of gamma-ray detection, particularly with the introduction of reverse-biased germanium detectors. These detectors can be arranged in geometric arrays to create a multi-detector system, enabling the detection of even the faintest transitions [54–56]. By employing a multi-detector array featuring N Compton-suppressed HPGe detectors, the number of two-fold events can be increased by a factor of $N(N-1)/2$. A multi-detector system greatly improves total photopeak efficiency and peak-to-background ratio. By using an extensive array of closely positioned detectors, gamma photons emitted from various directions can be detected simultaneously. This strategic arrangement covers nearly the entire 4π solid angle around the target, enabling accurate directional correlation ratios and precise polarization measurements for a deeper analysis of emitted gamma radiation.

2.4.1 HPGe Detector

The HPGe (high-purity Germanium) detector functions similar to the reverse-biased p-n junction semiconductor detectors. Here, the electric field in a depletion region removes charge carriers produced by incoming radiation. The width of this region is governed by $\sqrt{(V_{rev})/N}$ relation, where V_{rev} is the reverse-bias voltage and the impurity concentration is given by (N). "High purity" term is derived for the low concentration of impurity that is as low as 1 part in 10^{12}. This results in depletion widths of several centimetres.

The n-type detectors are generally preferred because they are less vulnerable to neutron damage and have thinner contacts, improving the detection of low-energy transitions. In order to reduce thermal electronic noise HPGe detectors operate at liquid nitrogen temperature (77 K). This ensures high resolution and sensitivity for nuclear measurements and gamma spectroscopy.

2.4.2 Compton Suppression Shield

Even though the resolution of HPGe detectors is commendable, the detectors lack good efficiency. As discussed earlier Compton effect is responsible for adding up the background to the spectrum, thereby reducing the peak-to-total ratio appreciably. Peak-to-total ratio (PT) for a detector is defined as :

$$PT = \frac{Total\ number\ of\ counts\ in\ photopeak}{Total\ number\ of\ counts\ in\ entire\ spectrum} \tag{2.8}$$

One way to counter the problem is to remove the Compton part by surrounding each HPGe detector with a shield of material, known as *anti-Compton shields* (ACS). The events detected in the detector and the shield simultaneously can be rejected electronically and it provides a veto for Compton scattered events. The process is termed as *Compton suppression*. The shield is in general made up of NaI(Tl) and BGO scintillator (Bismuth germanate). The detection efficiency is better in scintillation detectors. The suppressed peak-to-total ratio is around 50-60% compared to 20% for normal HPGe detectors. Fig. 2.3 shows a schematic diagram of the HPGe detector with a Compton suppression shield.

2.4.3 Resolving Power

The resolving power (R_p) of an array is the measure of its effectiveness in resolving sequences of γ transitions from a very complex spectrum. It is given by [56]:

$$R_p = (SE_\gamma/\Delta E_\gamma)PT \tag{2.9}$$

where SE_γ is the average energy separation between two transitions in a cascade. PT refers peak-to-total ratio. The energy resolution $\Delta {E_\gamma}^2$ of a detector is expressed as [56] :

Figure 2.3 Schematic diagram of HPGe detector with Compton suppression shield. Figure taken from Ref. [1].

$$\Delta E_\gamma{}^2 = (\Delta E_{int}{}^2 + \Delta E_{open}{}^2 + \Delta E_{ang}{}^2 + \Delta E_{vel}{}^2). \tag{2.10}$$

where ΔE_{int} is the intrinsic resolution of the detector whereas ΔE_{open}, ΔE_{ang} and ΔE_{vel} represent the effect of Doppler broadening on resolution due to opening angle of detector, angular spread of the recoil nuclei in the target and due to spread in velocity of recoiling nuclei, respectively.

2.5 Clover Detectors

To meet the increasing demand for higher efficiency detector systems without a loss in energy resolution, large-size HPGe single crystal detectors seemed to be a solution. But, it

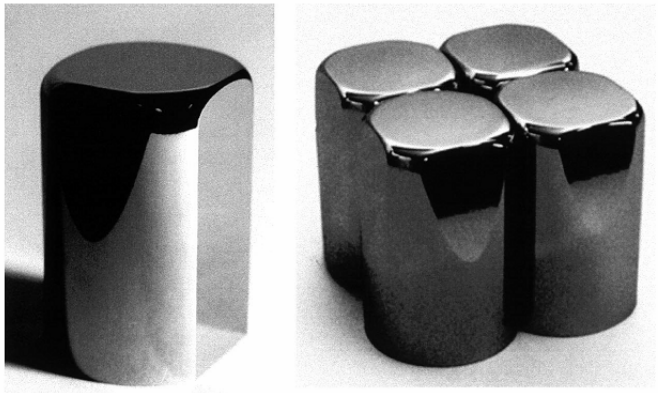

Figure 2.4 The left panel shows a single HPGe crystal, whereas the rightmost panel displays a closely packed arrangement of four crystals that form a clover. This figure is taken from Ref. [57].

had its own disadvantages. First of all, growing a large-sized crystal involves experimental constraints. Secondly, the time spread of charge collection over a large volume would deteriorate the timing characteristics of the detection system. With the increase in size of the crystal, the Doppler broadening in detected radiations would cause reducing the energy resolution of the system. The above-mentioned problems were solved with the introduction of a clover detector system [57, 58]. The composite system is the arrangement of four coaxial HPGe detectors placed side by side in the same enclosure. The four crystals are housed in a single cryostat which is in turn connected to a low-temperature FET coupled with a resistive charge-sensitive preamplifier. Each of these crystals generates independent energy and timing signals. The effective solid angle has been reduced by reducing the distance between the cap and the cryostat. The front face of the crystals is shaped in a quasi-squared section to enable close packing of the diodes with a minimal Ge-Ge distance. The crystals are held by the rear side in order to reduce the material surrounding the crystal, thereby improving the peak-to-background ratio [57, 59]. The design of the clover system is shown in Fig. 2.4. For high-energy γ rays, the effect of Compton scattering becomes a predominant factor. The use of clover enables recovery of the lost full-energy due to Compton scattering by a time-correlated addition of energy signal in all four crystals. The

mode is known as $Addback-mode$. Furthermore, the clover composite can also be used as a polarimeter. A comparison of efficiency corrected intensity across horizontal and vertical scattering proves to be helpful in determining the electric or magnetic nature of radiation.

2.6 Indian National Gamma Array (INGA)

The Indian National Gamma Array (INGA) has been set up at T.I.F.R.-Mumbai. A maximum of 24 clover detectors can be accommodated in the array which is designed with spherical geometry. The detectors were mounted at seven angles, with six detectors at 90° position and three clovers each at 23°, 40°, 65°, 115°, 140° and 157°. The target-to-crystal distance is 25 cm. The overall photopeak efficiency is $\sim 5\%$ at the energy of γ-transition of 1 MeV. A peak-to-total ratio of $\sim 40\%$ has been obtained in Compton suppressed data for ^{60}Co in addback mode. The energy resolution for a single crystal of a clover comes out to be 2.2 keV at 1.33 MeV γ-ray energy [60–62]. It is also possible to mount ancillary detectors such NaI(Tl) multiplicity filters or CsI(Tl)/Si charged particle and $LaBr_3$ detectors with the pre-existing clovers in the array. The INGA set-up is shown in Fig. 2.5.

2.7 Signal Processing

The working of traditional signal processing involving analog hardware is described in brief below. The signals received from the detectors are passed through a pre-amplifier which extracts two identical signal pulses from each detector; one of which gives the amount of energy deposited and the other will be used to determine when the energy is deposited. These pulses, in turn, are passed through the amplifier. Distortion effects like $walk$ and $time-jitter$ are produced within the original signal. $Constant\ fraction\ discriminator$ or CFD is used to remove $walk$. Optimization of the pulse signal is carried

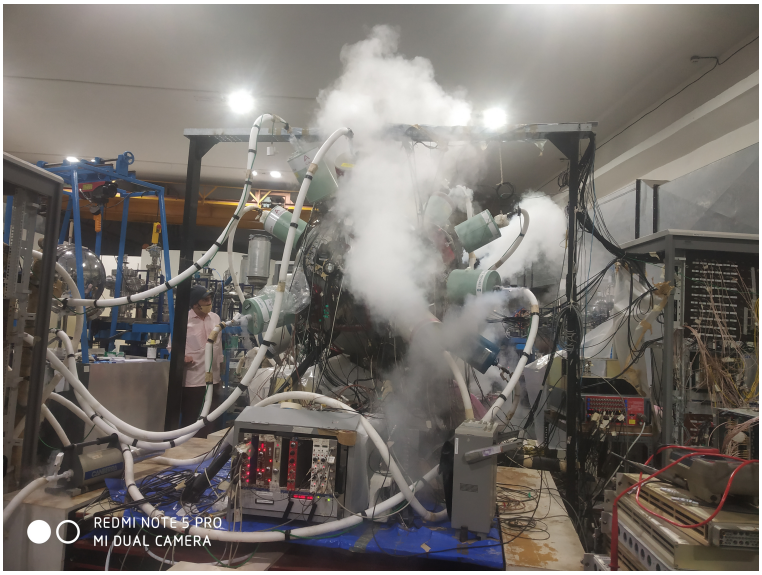

Figure 2.5 INGA set up at T.I.F.R. Mumbai.

out with the help of a number of filters with a small time constant which gives a pulse with a very short rise and fall time; this helps in improving the time definition and reducing the noise factor. These modules are followed by *coincidence unit* or *CU*. The width of the coincidence window is set by using the *CU*. If the two pulses arrive within this time interval/time window, the emission of both gamma quanta is said to happen promptly. Ideally, a prompt emission of two gamma quanta should give time signals from each detector that are simultaneous but because of jitter this time is reduced, some coincident gamma pairs will be lost, and if it is too long, the number of random coincidences will increase. When both the input signals to the *CU* are active, *CU* will give a logic pulse, just like a normal AND gate. However, present day's arrays mostly implement digital signal processing which we discuss in the next sections.

2.7.1 Analog to Digital Converter (ADC)

The basic function of an *ADC* is to produce a digital code at its output that is proportional to an analog voltage supplied to its input. The ideal *ADC* would perform a perfectly linear

conversion of analog voltage to a code value. Due to the discrete nature of the output, input voltage spans over a small range of values. Hence, a plot of the midpoint of the range of input values vs output code number will be best fitted by a straight line. The integral linearity specification for the *ADC* is generally quoted as the maximum deviation of the measured curve from the best fit straight line expressed as a percentage of the full range value [63, 64].

2.8 Electronics for INGA

A digital data acquisition system has been implemented at INGA [62, 65]. Compared to the analog acquisition systems, digital counterparts provide compactness, a versatile nature and budget effectiveness. Moreover, it facilitates the acquisition and storage of waveforms on an event-by-event basis. The present requirements demand information about energy and timing signals from the 96 channels of the 24 clovers vetoed with corresponding Compton suppressors, BGO shields. Other requirements of fast timing, zero dead time, and coupling of ancillary detectors with clovers, which should be taken care of by the digital acquisition system. Pixie-16 module with PCI-PXI based architect of the XIA LLC [66] has been implemented for the present INGA set-up. A block diagram of the modules is shown in Fig. 2.6. The system consists of six Pixie-16 modules, two LVDS (Low Voltage Differential Signalling) level translator modules and one controller arranged in a single Compact PCI/PXI crate. Each Pixie-16 module is designed for 16 input channels to serve four clovers. The Pixie-16 module receives a preamplifier signal which is digitized with 12-bit FADC (Flash Analog to Digital Converter) at a rate of 100 MHz. The stream of digitized data in turn produces a fast trigger signal when the fast trapezoid filter output crosses a predefined threshold. One of the six cards acts as the Director, which receives and redistributes trigger signals among all the remaining cards. Furthermore, the Director is responsible for computing total multiplicity as well as opening the coincidence time

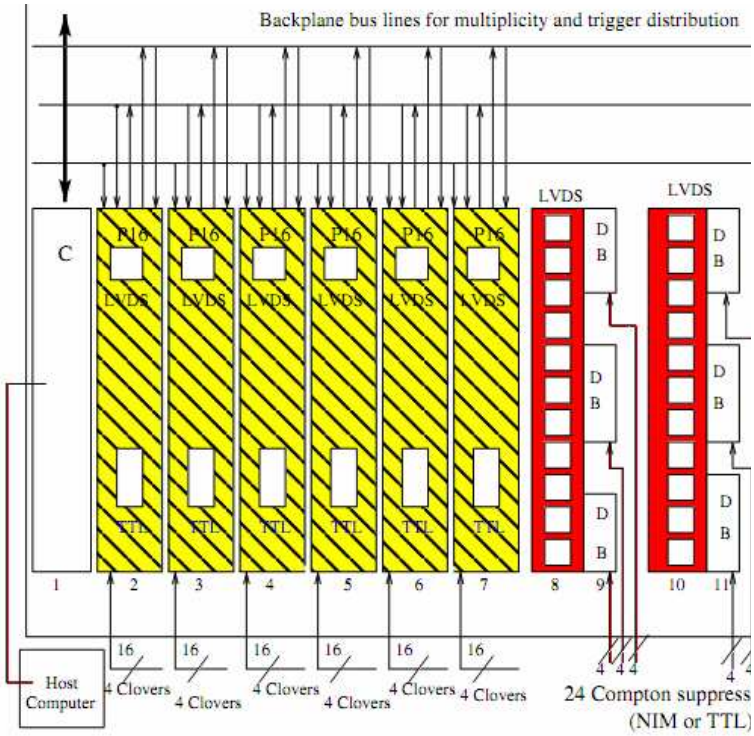

Figure 2.6 Block diagram of Pixie-16 module. Figure taken from Ref. [62].

window. For BGO shields, a logic signal is generated through conventional fast trigger circuits using TFA and CFD. The signal is in turn, fed to Pixie-16 modules for veto. In the absence of any veto signal, a fast trigger produces a valid signal. For each valid signal from preamplifier, energy information is obtained through on-board digital processing of the pulse shape, and timing is measured by latching the clock with the arriving pulse. The crate is connected to a PC through an optical bridge. The data acquisition is monitored by PC which looks for the FIFO (first in, first out) across each module. Once FIFO is ready, the data is transferred to the PC. All the modules in the digital system are synchronized with respect to the precision defined by the clock. Subsequently, the list mode data for each module is written in separate files in the hard disk. The time-stamped data from different modules are collected to generate a merged single data stream as per 48-bit 100 MHz time-stamp and event number. For analysis, the merged data were sorted using the “Multi

pARameter time-stamp-based COincidence Search program (MARCOS)" developed at T.I.F.R [62].

2.9 Data Processing

The "Data Processing" section can be categorized into two sections : (a) $pre-sorting$ of data which comprises of gain matching, energy and efficiency calibrations, add-back procedure etc. (b) Data *compression*, which includes rejection of unwanted events to create a more compact data format which is smaller in size compared to the raw data and easier to handle. The final format of data contains information of detector identification numbers, γ-ray energies, timing information of arrival of photons and multiplicity.

2.9.1 Energy and Efficiency Calibration

The energy of incident γ photons is processed in the preamplifier, amplifier and *ADC*s or are digitally processed, where the channel number is proportional to γ-ray energy. Usually, each detector has different sets of gain parameters; hence, standard radioactive sources have to be used to standardize the detectors/crystals in terms of gain parameters. Such sources are ^{152}Eu and ^{133}Ba for the low-medium energy regime of the spectrum, whereas ^{56}Co is used for high energy transitions. The centroid of each peak is determined in terms of channel number in the detector/crystal, and the known energies are fitted against the channel numbers using a polynomial fit based on:

$$E_\gamma = \sum_{n=1}^{k} (c + m_n x^n). \tag{2.11}$$

where x is the channel number, E_γ is measured in keV, c and m_n are the calibration coefficients and n is the degree of polynomial. A quadratic fit is sufficient to calibrate the detectors. The coefficient "c" basically gives the offset value. The first order coefficient

which gives an estimate of the gain of amplifier, whereas the coefficient to the second order term is a measure of non-linearity in the detection set-up. Furthermore, the gain may not be stable over the time span of a few days of experiments, and electronic instability may lead to fluctuations in gain for detectors/crystals. Therefore, it is advisable to get the gain parameters of detectors/crystals with a set of data collected at different times during the experiment. The efficiency parameter, i.e., how many photons are detected with respect to either those emitted by the source or incident on the detector, is unique to each detector/crystal. Therefore, in order to measure relative intensities of the observed transitions, it is required to have efficiency correction across the entire set-up of detectors. For this purpose, known sources with properly measured relative intensities are used to compare the relative intensities in the given system. The efficiency ε, can be correlated to the E_γ through the following relation [67]:

$$ln(\varepsilon) = [(A + Bx + Cx^2)^{-G} + (D + Ey + Fy^2)^{-G}]^{-1/G}. \quad (2.12)$$

where $x = ln(E_\gamma/100keV)$ and $y = ln(E_\gamma/1000keV)$. The coefficients A, B and C are useful for low-energy transitions whereas E, F and G are effective for higher energy γ rays. The parameter G acts as a bridging factor between high and low energy regions. The higher the value of G, the sharper will be the turnover at the top of the peak. A typical example of efficiency vs E_γ plot extracted from the experiments at TIFR Mumbai is shown in Fig. 2.7.

2.9.2 Data Analysis

Data sorting

In order to probe into the nuclear structural property, meaningful sorting of data is required. The most preliminary type of sorting is to generate a one-dimensional histogram with

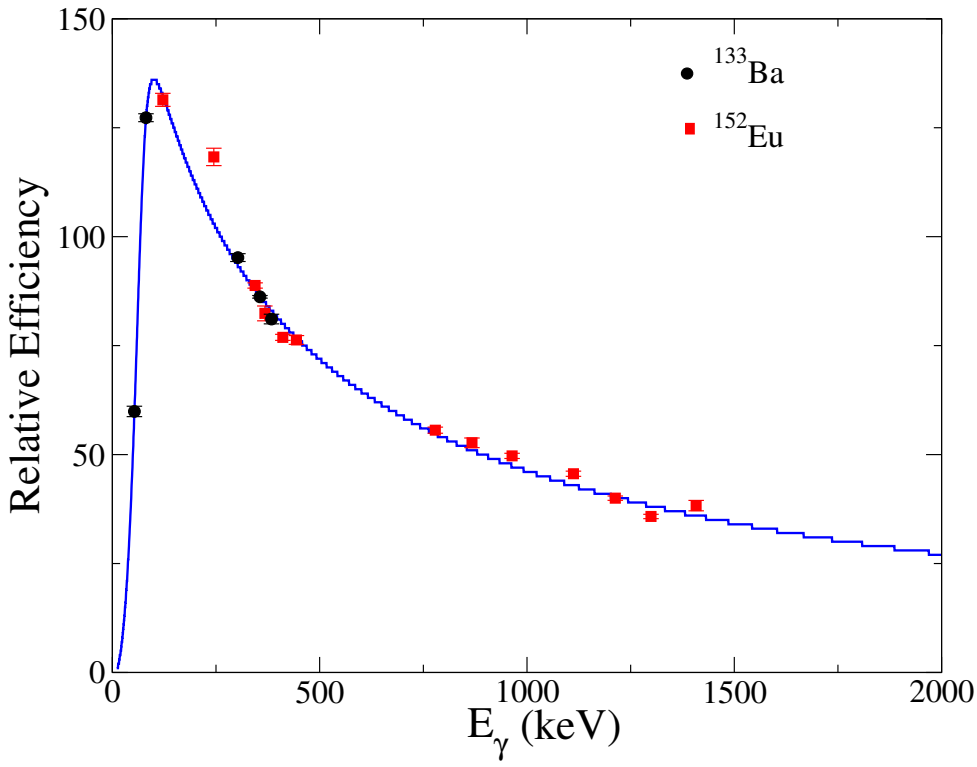

Figure 2.7 Relative efficiency curve vs energy of transition for all detectors of INGA set up.

energies of transitions on one axis and the corresponding counts on the other one. This is a spectrum with no implemented constraint and displays all the energy peaks (irrespective of populated channels) across every populated channel. Therefore, it is called a *total projection*. Higher dimensional histograms (matrices, cubes and hypercubes) can be generated for higher fold events. To begin with, two or higher-fold coincidence data can be analyzed with a two-dimensional histogram, often called a γ-γ matrix. The γ-ray energies are used in both the axes, say x and y. The third axis, say z, contains the corresponding counts. Each event is unfolded into pair of energies $(E_\gamma^{x_i}, E_\gamma^{y_i})$ and bins corresponding to $E_\gamma^{x_i}$ and $E_\gamma^{y_i}$ are incremented. Matrices have advantage over one-dimensional spectrum that a single gate can be set on one of the energies or a list of energies on one axis and the spectrum can be obtained by projecting the data on the other energy axis. On the same footing, cube and hypercubes can be constructed for three and higher as well as

four and higher fold data [67]. As the high-fold histograms are created, the corresponding number of events of γ rays decreases owing to the fact that events are distributed over extra dimensions and the lower-fold events are rejected. The high-fold events can always be decomposed into subsequent lower fold events, where the fold of the sub-events is dependent on the dimension of the considered historgram [68]. Coincidence relationship between the transitions, observation of branching out or feeding in transitions and their relative intensities would be helpful in building up the level scheme with the strongest transition at the bottom and subsequent transitions to follow. In order to determine the relative intensity of a transition, it is customary to normalize its intensity with respect to one of the lower transitions which is not contaminated from the population of other channels. The package Radware [67] has been used for data analysis in the present thesis.

2.9.3 Angular Distribution

Multipole character of a γ radiation can be determined using angular distribution measurement of the γ transition. In a fusion-evaporation reaction, the angular momentum vector of the compound nucleus is aligned to a direction perpendicular to the projectile (beam) axis [69, 70]. The effect results in unequal population probability $p(m_i)$ of a substate m_i which is governed by Gaussian distribution centered around $m = 0$ substate of a given spin I [71–73]:

$$p(m_i) = \frac{\exp(-m^2/2\sigma^2)}{\sum_{m'=-I}^{I} \exp(-m'^2/2\sigma^2)}. \tag{2.13}$$

where σ is the half-width. It is usually given as σ/I. For the completely aligned case, the value of σ tends to zero. In general, the angular distribution probability of multipole radiation, $W(\theta)$, when a γ radiation is emitted out in a direction θ to the beam axis, is given in terms of even powers of $\cos\theta$:

$$W_l(\theta) = \sum_{k=0}^{l} A_{2k} P_{2k}\ (cos\theta) = A_0 + A_2 P_2\ (cos\theta) + A_4 P_4\ (cos\theta) + ... + A_{2l} P_{2l}\ (cos\theta) \tag{2.14}$$

The coefficients A_{2k}'s are the angular distribution coefficients that depend on the degree of alignment and spins of the corresponding states and multipole order of the transitions, respectively. The distribution is based on Legendre polynomials, $P(\theta)$. To fulfil the conservation of parity, the value of k obeys $k < 2L$, L is the angular momentum taken away by the emitted photon. During the decay of a nucleus, the predominant order of multipole is either dipole or quadrupole. Therefore, it is sufficient to assume terms up to second order, i.e., k = 4.

$$W(\theta) = A_0 + A_2 P_2(\cos\theta) + A_4 P_4(\cos\theta) = A_0[1 + a_2 P_2(\cos\theta) + a_4 P_4(\cos\theta)] \tag{2.15}$$

We can obtain the angular distribution coefficients A_0, A_2 and A_4 (A_0, a_2 and a_4) by measuring the intensity of the γ ray at different angle θ with respect to the beam axis. The coefficients, A_{2k}, can be determined experimentally by fitting the intensities of desired transitions as a function of detector angle θ.

An example of angular distribution measurement using INGA (TIFR Mumbai) set up for a dipole transition (ΔI = 1) of energy 322.2 keV in ^{92}Nb with an energy of transition 322.2 keV is shown in Fig. 2.8. W(θ) is the efficiency-corrected counts for the mentioned transitions across different orientations [62, 74].

2.9.4 ADO-ratio of the γ -ray transitions

The multipolarities of the γ rays can be determined from the angular distribution of oriented nuclei (ADO) ratios [75]. This method is advantageous for transitions where DCO ratios

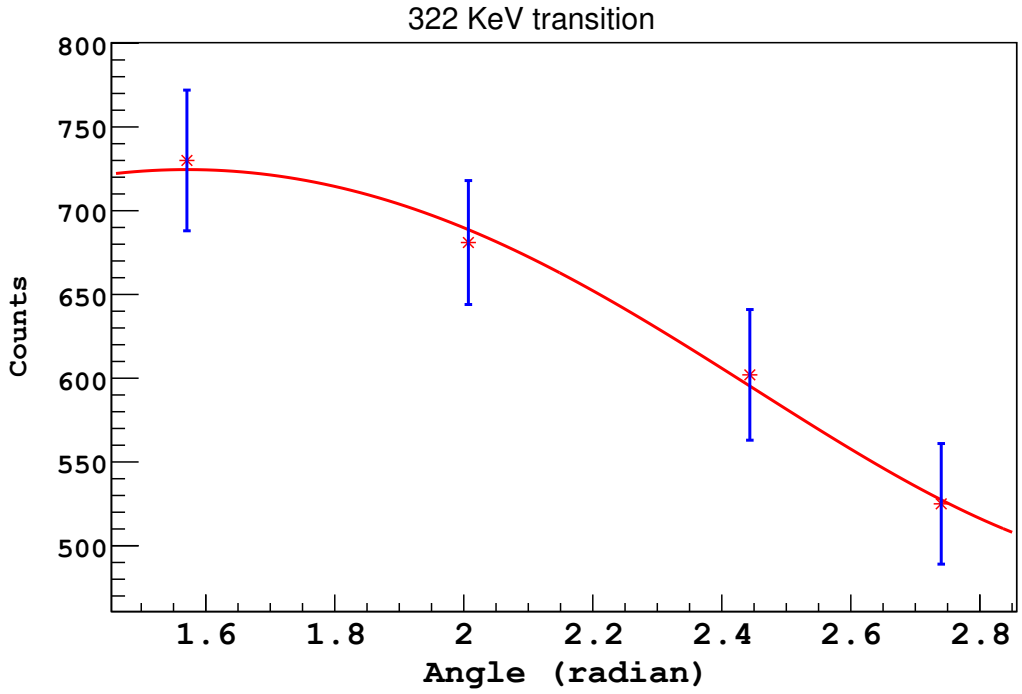

Figure 2.8 Angular distribution for a dipole transition in ^{92}Nb with a energy of transition 322.2 keV.

cannot be established due to poor statistics or lack of pure gating transitions, common in spherical or weakly deformed nuclei near shell closure, which interests this thesis. For ADO measurements, two asymmetric matrices were created. One contains events with γ-rays detected at 140° on one axis and counts in all detectors on the other, while the second matrix comprises counts detected in detectors at 90° on one axis and those in all detectors on the other. The intensity ratio is expressed as:

$$R_\theta = \frac{I_\gamma(\gamma 1^{157^\circ}, \gamma 2^{all})}{I_\gamma(\gamma 1^{90^\circ}, \gamma 2^{all})} \tag{2.16}$$

differentiates between a pure, stretched dipole($\simeq 0.7$) and stretched ($\Delta I = 2$) quadrupole ($E2$) ($\simeq 1.4$) transitions respectively when measured in a gate made on a quadrupole transition.

2.9.5 Linear-Polarization Measurement and Analysis

The use of Clover detectors in INGA set-up facilitates linear polarization measurement of γ radiations which is an effective tool for distinguishing between electric and magnetic transitions. The four crystals of clover detectors are used as Compton polarimeters. One of the crystals acts as a scatterer whereas the adjacent horizontal and vertical crystals play the role of observers [57, 76]. The process is called as polarization directional correlation (PDCO). Mostly, detectors at 90° are used for the purpose, such as in INGA. The method is based upon the fact that the direction of Compton scattered polarized photon is different for electric and magnetic transitions. Alternatively, the approach of integrated polarization-directional correlation (IPDCO) from aligned nuclei can be applied [57, 76]. In this method, two asymmetric matrices are sorted, each containing a number of γ photons scattered in a perpendicular and parallel direction to the emission plane on one axis and a coincident γ ray on the other axis, respectively. The asymmetry parameter is defined as [76]:

$$\Delta_{asym} = \frac{aN_{\perp} - N_{\parallel}}{aN_{\perp} + N_{\parallel}} \tag{2.17}$$

where $N_{\perp}$ and $N_{\parallel}$ are the numbers of scattered photons in a direction perpendicular and parallel to the direction of the reaction plane. The correction factor a is defined as [76]:

$$a = \frac{N_{\parallel}}{N_{\perp}} \mid_{unpolarized} \tag{2.18}$$

and can be evaluated from the asymmetry of γ rays from known unpolarized radioactive sources (^{152}Eu, ^{133}Ba) for which a value close to unity is obtained (see Fig. 2.9). The Δ_{asym} is either positive or negative, depending on the nature of the transition, whether it is electric or magnetic, respectively. A value close to zero indicates a possible admixture.

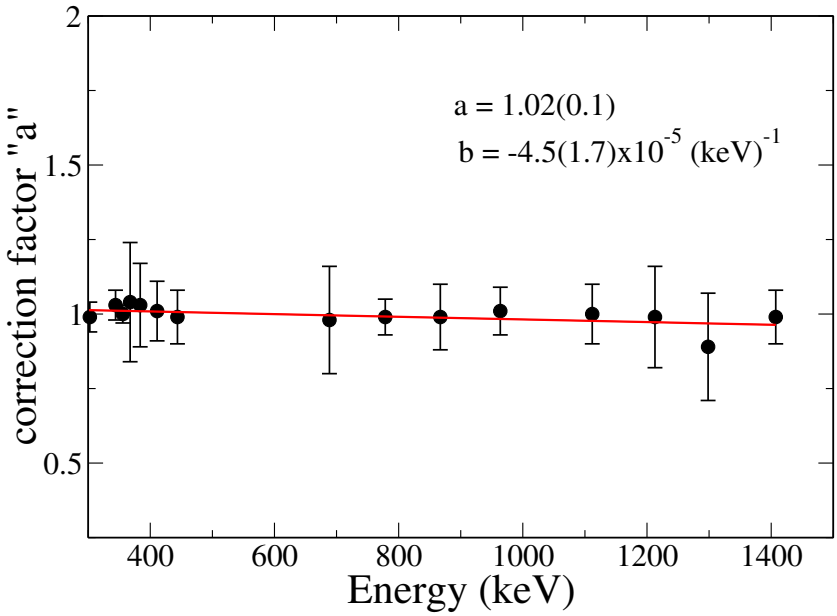

Figure 2.9 The asymmetry factor as a function of γ-ray energies for INGA set up at TIFR.

2.10 Determination of level Lifetime of the excited state

Measuring the lifetimes of excited states in nuclei is a highly active field in nuclear structure physics. In recent decades, precise lifetime measurements have provided essential insights into nuclear states, significantly enhancing our comprehension of nuclear structure.

The method used to obtain the nuclear level lifetimes of the excited states depends on the expected time range. For very short lifetimes $\approx 10^{-12}$ - 10^{-15} s, e.g. relevant for the collective high spin states, the Doppler Shift Attenuation Method (DSAM) is a widely used technique. The basic method of the DSAM technique is illustrated in Fig.2.10. For the lower spin states, longer lifetimes in the order of 1 - 100 ps are expected. In this case, the Recoil Distance Method (RDM) can be used to determine the lifetimes.

Electromagnetic radiation emitted from an excited nucleus, recoiling with velocity v, will undergo a shift in energy known as the Doppler shift. The shifted energy (E_γ) of the γ photon (in the laboratory frame of reference) can be expressed as,

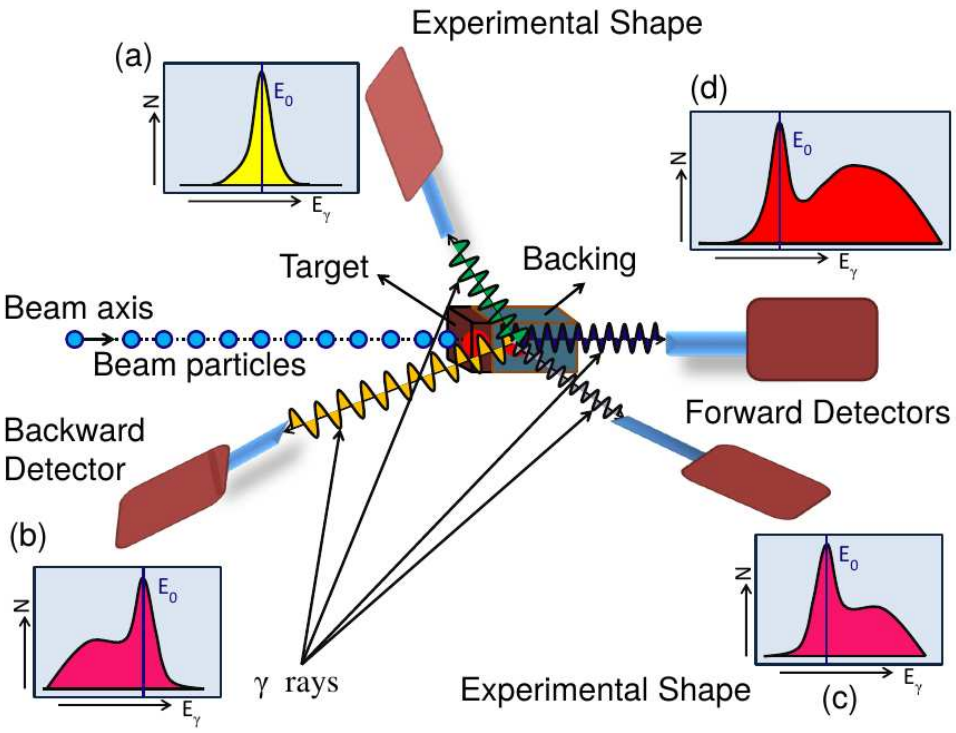

Figure 2.10 Schematic diagram shows the experimental lineshape of a transition decaying from a state whose level lifetime $\sim$ 1 ps. The resulting γ-ray Doppler shift as observed by the detectors placed at (a) a backwards angle (θ) close to 90°, (b) a backwards angle θ, $180° > \theta > 90°$, (c) an forward angle θ, $90° > \theta > 0°$, and (d) forward angle $\theta = 0°$ [77].

$$E_\gamma = E_\gamma^0 \frac{\sqrt{1-v^2/c^2}}{1-(v/c)cos\theta} \simeq E_\gamma^0(1+\beta cos\theta) \tag{2.19}$$

[for small β]

where E_γ^0 is the energy of the unshifted γ-radiation and β (= v/c) is the velocity of recoil in unit of c. Here, θ is the angle between the direction of γ ray emission and the velocity of the recoiling nucleus.

The reaction which forms the excited recoiling nuclei needs to be chosen in such a way that, ideally, the residual nuclei should recoil in one direction with a unique velocity only. In the actual experiment, one normally ensures that the nuclei recoil in a narrow cone centred with respect to the beam direction. A beam of incoming particles hits the target nuclei and forms a compound nucleus. Reaction products (protons, neutrons and/or α

particles and γ rays) are emitted and left the final residual nucleus in an excited state. The initial velocity (v_0) of the residual nuclei slows down due to the number of collisions with the electron and/or nucleus in the target and/or target-backing combination. During the slowing down process, a γ ray is emitted after a time related to the mean lifetime (τ) of the excited state. The mean velocity of recoil at that time has dropped to v. The quantity v is determined experimentally by measuring the average Doppler shift of the emitted γ ray. Using Eq. (2.20) by measuring the centroid of the shifted shape the average velocity of the recoil nuclei (v_{av}) when they emit γ ray can be determined. The attenuation factor F (τ) and the level lifetime (τ) of the excited state are related through the following relation,

$$F(\tau) = \frac{v_{av}}{v_0} = \frac{1}{v_0 \tau} \int_0^\infty v(t) e^{-t/\tau} dt \tag{2.20}$$

where, v_{av} and v_0 are the average velocity of the recoiling nuclei when the γ rays were emitted and the initial velocity, respectively. Once the attenuation factor multiplied by v_0 is obtained the slowing down process for the recoils is simulated using Monte-Carlo techniques [78]. The lifetime is then obtained by comparing the experimental data with these calculations. If the lifetimes of the states of interest are not short compared to the average stopping time of recoils, then the velocity of recoils becomes close to zero at the time of γ -ray emission. However, the de-exciting γ rays are emitted during the slowing down process inside the target-backing combination and depending on the velocity distribution of these γ rays the level lifetime may be deduced by performing lineshape analysis.

2.10.1 Lineshape Analysis

The level lifetimes of the states have been extracted by fitting these line shapes using the LINESHAPE analysis code [79, 80]. It consists of three sub-programs: dechist, histaver and lineshape. Dechist simulates the velocity histories of the recoiling nuclei through the

target and backing medium using the Monte Carlo technique. The slowing down history of 10,000 recoil nuclei, traversing the target and the backing media, has been simulated by the Monte Carlo techniques with a time step of 1.5 fs. The shell corrected stopping powers of Northcliffe and Schilling [78] have been used for these calculations. These histories have been used to generate angle-dependent velocity profiles for detectors at different angles, wherein the clover geometry of the detector has been used as an input. The velocity profiles have been used to calculate Doppler shapes for the γ-ray transitions of interest. The experimental spectra, showing the shape of the transitions of the band of interest, have been constructed. The lifetimes for the states in the band have been extracted by least-squares fitting of the calculated shapes to the experimental (gated) spectra. The gate on the transitions below (GTB) the transitions of interest necessitate considering the side-feeding contribution, which can be ruled out by setting a gate on the top. In the case of the GTB, side-feeding has been modelled with a cascade of five transitions and having a moment of inertia the same as that of the band under consideration. Initially, starting from the topmost transition, the members of the band have been sequentially fitted. A direct feeding has been assumed to calculate the shape for the transition from the topmost level, for which a clear line shape has been observed. This gives us the value of the effective lifetime of the state. For the subsequent transitions in the band, the transition quadrupole moment, the side-feeding quadrupole moment, the peak height and the background have been used as the free parameters for the least square procedure. Following a satisfactory fit, the spectrum parameters like the peak height and the background have been fixed at the corresponding values. After having fitted all the transitions of the band, sequentially, a global least squares minimization has been carried out for all the transitions of the cascade, simultaneously, wherein only the transition quadrupole moment and the side-feeding quadrupole moments for each state have been kept as free parameters. The gates have been set on the transitions below the band of interest. In the present experimental setup, the

spectra at 65°, 90° and 140° have been fitted simultaneously to extract the level lifetimes. Uncertainties in the lifetimes have been derived from the behavior of the χ^2 fit in the vicinity of the minimum. The quoted errors in the lifetime do not include the systematic errors due to the uncertainty in the stopping power which can be as large as 15%.

2.10.2 Lifetime from Time Difference Spectrum

The mean lifetime of an excited state can be estimated by measuring the average time difference between the prompt gamma rays feeding to the state of interest and the delayed γ rays de-exciting through the state. The time difference spectrum between two transitions $E1$ and $E2$ in a cascade (Fig.2.11) can be obtained from the list mode data using the following procedure. Four conditional time spectra T_{P_1,P_2} , T_{P_1,b_2} , T_{b_1,P_2} and T_{b_1,b_2} need to be generated from the time-stamped data. The pictorial representation of this is shown in Fig.2.11. Here, T_{P_1,P_2} is the time difference spectrum obtained from the energy gate around the peaks P_1 (115.4-keV) and P_2 (2211.0-keV), while T_{P_1,b_2} represents the same for energy gate around the P_1 peak and background near P_2 peak. Similarly, the third and fourth spectra are for background-peak and background-background spectra. The final time difference spectrum has been constructed by using the relation [62],

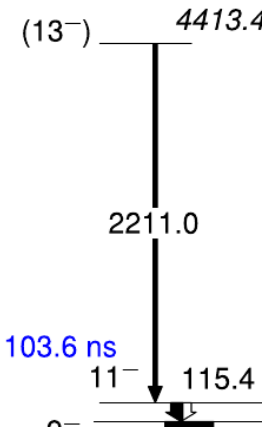

Figure 2.11 Construction of the time difference spectrum between two γ rays feeding (2211.0-keV) and de-exciting (115.4-keV) through the state of interest (11^-) [81, 82].

$$T = T_{P_1,P_2} - T_{P_1,b_2} - T_{b_1,P_2} + T_{b_1,b_2} \tag{2.21}$$

The time-difference spectrum was generated using 2211.0-keV transition as a "start", whereas 115.4-keV γ ray below the isomeric state at 11^- as a "stop". The fitted curve is shown in Fig. 6.8. Data fitting has been done using the ROOT software packages [83]. The half-lives of the states were extracted by fitting the time-difference spectra with convoluted Gaussian and exponential functions, considering the detector response function as explained in ref. [84, 85]. The expression is as follows:

$$I(t) = Aexp\left(\frac{\sigma^2}{2\tau^2} - \frac{t}{\tau}\right)\left[1 - erf\left(\frac{\sigma^2 - \tau t}{\sqrt{2}\sigma\tau}\right)\right] \tag{2.22}$$

where A is the intensity normalization constant, t corresponds to the time difference since the defined time zero, τ defines the mean-lifetime of the decaying state, σ represents the Gaussian standard deviation, and $erf()$ is the error function. The half-life of the 11^- state has been measured to be 103.6(32) ns.

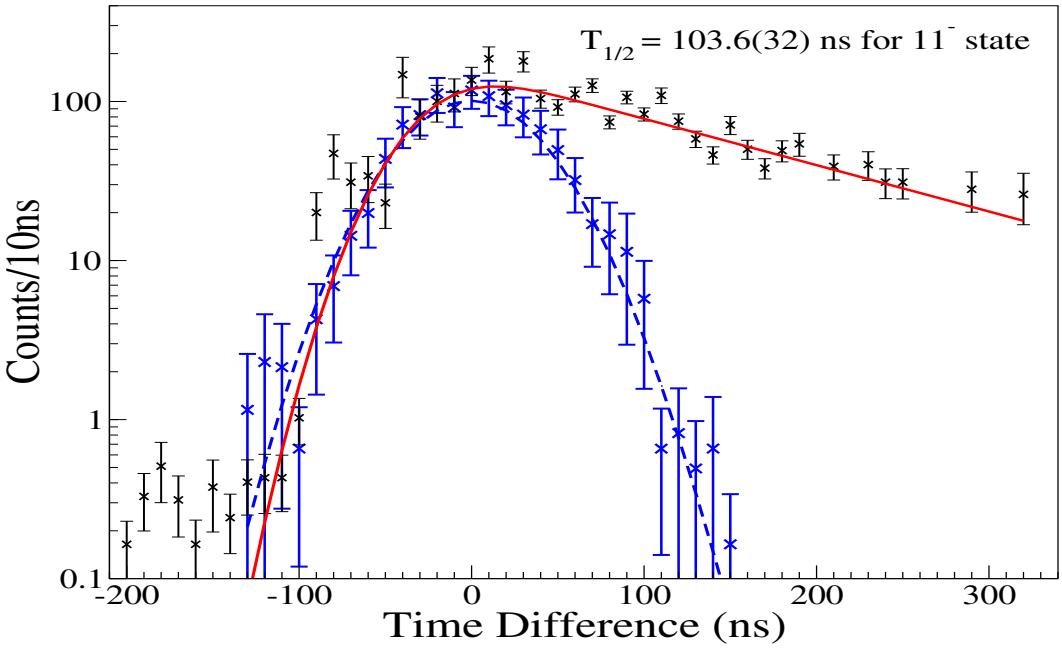

Figure 2.12 The time-difference spectra were constructed from the present data on ^{92}Nb using the 2211.0-keV transition as a "start" and the 115.4-keV transition below the isomeric level as "stop". The solid red line, showing the fitting to the selected portion of the experimental spectrum by fitting a convoluted Gaussian and exponential function to the time difference spectrum, gives a half-life of 103.6(32)ns. The prompt was constructed with the coincidence of 327.7 and 2286.6 keV transitions as "start" and "stop", respectively. The prompt curve is fitted with the Gaussian function and is displayed by the blue color solid line. The blue Gaussian curve is used as a representative plot to compare the shape of the time spectrum between the prompt and the delayed peak. The prompt curve y-axis is scaled down by a factor of ~ 6. The prompt curve has not been used to fix the Gaussian width of the fits across the delayed curve. It is hereby mentioned that the data points from -120 ns to -200 ns have been considered for the fitting of the delayed curve.